HIA: A Hybrid Integral Approach to model incompressible isotropic hyperelastic materials - Part 1: Theory

Alain Nguessong Nkenfack, Beda Tibi, Zhi-Qiang Feng, François Peyraut

HIA: A Hybrid Integral Approach to model incompressible isotropic hyperelastic materials—Part 1: Theory

A. Nguessong Nkenfack [a,b,*], T. Beda [b], Z.-Q. Feng [c,d], F. Peyraut [a]

[a] *IRTES-M3M, UTBM, UBFC, 90010 Belfort Cedex, France*
[b] *Faculty of Sciences, University of Ngaoundéré, Cameroon*
[c] *School of Mechanics and Engineering, Southwest Jiaotong University, Chengdu, China*
LMEE, Université d'Evry, Evry, France

This paper provides a new constitutive model for rubber-like materials. The model adds to the 8-chain density introduced by Arruda and Boyce, two phenomenological components: an original part made of an integral density and an interleaving constraint part represented by a logarithmic function as proposed by Gent and Thomas. The model contains six rheological parameters connected to the polymer chemistry and to the macroscopic behavior. Four sets of experimental data from the literature are used to identify the rheological parameters and to assess the proposed model. The model is able to reproduce with a good accuracy experimental data performed under different loading conditions such as uniaxial and equibiaxial tension, uniaxial compression, pure and simple shear as well as the Mooney plot.

1. Introduction

Rubbers and elastomers are used in various applications such as seals, tires or vibration mounts. Their chemical and mechanical properties make them good sealing elements against humidity, pressure and temperature. They possess in addition very good properties of energy absorption. Industrial use of rubber requires characterizations that need modeling behavior and a very large variety of models was proposed to this purpose in the literature during the last sixty years [1–13].

Several constitutive models are based, for example, on the statistical mechanics as the neo-Hookean strain energy deduced from the Gaussian law [14–16] or on the strain energy of polymer chains using the Langevin statistics [1,2,5,12,17,18].

In addition to the statistical mechanics-based models mentioned above, it exists many phenomenological models for rubber materials in the literature, see for example the reviews of Steinmann et al. [18] and Marckmann and Verron [19] on this topic. According to the models developed by Mooney [4], Yeoh [8], Gent [20], Pucci and Saccomandi [21] and Beda [10,22], the strain energy of rubber material can be expressed with respect to the invariants of the strain tensor. Alternatively, the models suggested by Valanis and Landel [23], Ogden [6] and Davidson and Goulbourne [12] are expressed according to the principal stretches of the strain tensor. However, these models present difficulties to predict the behavior of the material for large compressive loading, particularly in the case where the Mooney plot is used to represent the experimental data [24].

In this context, we propose a new constitutive model for rubber materials which attempts to reconcile basic concepts from the molecular and phenomenological theories of hyperelasticity. This model is based on the 8-chain energy density introduced by Arruda and Boyce [1] to predict the affine deformation of the molecular chain [2]. It also includes the logarithmic function suggested by Gent and Thomas [3] to model the interleaving of the molecular chains. Finally, it includes two original contributions:

1. An integral density allowing an excellent fit of the experimental data for large compressive loading.
2. A new accurate computation of the inverse of the Langevin function to well describe the affine part of the rubber behavior [25].

In this way, the new model can be regarded as an hybridization between the molecular and the phenomenological theories. It contains six rheological parameters that need to be determined on the basis of experiments. Once these rheological parameters have been identified, the model was successfully compared to

* Corresponding author at: Faculty of Sciences, University of Ngaoundéré, Cameroon.
E-mail addresses: nguessong.alain@yahoo.com (A. Nguessong Nkenfack), zhi-qiang.feng@ufrst.univ-evry.fr (Z.-Q. Feng).

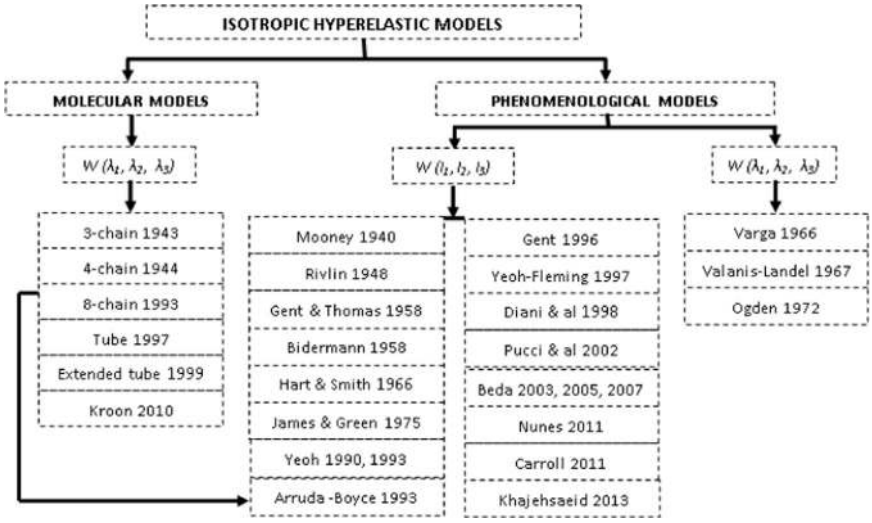

Fig. 1. Summary of a few isotropic energy densities.

experimental data from the literature [1,26–28] providing a remarkable agreement with the compressive part of the Mooney plot.

2. Hyperelastic constitutive laws – State of the art

This section is divided into two parts where some basics of the theory of hyperelastic models are reminded. The first part gives a brief description on kinematics, while the second one reminds the most popular isotropic hyperelastic models used during the six last decades.

2.1. Kinematic tensors

The second Piola–Kirchhoff stress tensor $\mathbf{S}$ is classically written as the derivative of the energy density W with respect to the Green–Lagrange strain tensor $\mathbf{E}$, or to the right Cauchy–Green strain tensor $\mathbf{C}$:

$$\mathbf{S} = \frac{\partial W}{\partial \mathbf{E}} = 2\frac{\partial W}{\partial \mathbf{C}} \tag{1}$$

$$\mathbf{E} = \frac{1}{2}(\mathbf{C} - \mathbf{I}); \quad \mathbf{C} = \mathbf{F}^T\mathbf{F}; \quad \mathbf{F} = \mathbf{I} + \frac{\partial \mathbf{u}}{\partial \mathbf{X}} \tag{2}$$

where $\mathbf{F}$, $\mathbf{I}$, $\mathbf{X}$ and $\mathbf{u}$ are respectively the deformation gradient matrix, the identity tensor, the Lagrange coordinates and the displacement vector.

For isotropic materials, the energy density W depends on the three principal invariants of $\mathbf{C}$ [29,30]:

$$I_1 = \mathrm{tr}(\mathbf{C}); \quad I_2 = \frac{1}{2}[(\mathrm{tr}\mathbf{C})^2 - \mathrm{tr}(\mathbf{C}^2)]; \quad I_3 = \det(\mathbf{C}) \tag{3}$$

where tr and det represent respectively the trace and the determinant of the matrix. It is classically deduced from Eqs. (1) and (3) that:

$$\mathbf{S} = 2\sum_{i=1}^{3}\frac{\partial W}{\partial I_i}\frac{\partial I_i}{\partial \mathbf{C}}; \quad \frac{\partial I_1}{\partial \mathbf{C}} = \mathbf{I}; \quad \frac{\partial I_2}{\partial \mathbf{C}} = I_1\mathbf{I} - \mathbf{C}; \quad \frac{\partial I_3}{\partial \mathbf{C}} = I_3\mathbf{C}^{-1} \tag{4}$$

or equivalently:

$$\mathbf{S} = 2\left[\left(\frac{\partial W}{\partial I_1} + I_1\frac{\partial W}{\partial I_2}\right)\mathbf{I} - \frac{\partial W}{\partial I_2}\mathbf{C} + I_3\frac{\partial W}{\partial I_3}\mathbf{C}^{-1}\right] \tag{5}$$

The standard relationship between $\mathbf{S}$ and the Cauchy stress tensor $\boldsymbol{\Sigma}$ is recalled:

$$\boldsymbol{\Sigma} = \frac{1}{\sqrt{I_3}}\mathbf{F}\mathbf{S}\mathbf{F}^T \tag{6}$$

By using the Cayley–Hamilton theorem, a straightforward computation from (5) and (6) gives:

$$\boldsymbol{\Sigma} = \delta_1\mathbf{I} + \delta_2\mathbf{B} + \delta_3\mathbf{B}^{-1} \tag{7}$$

where $\mathbf{B} = \mathbf{F}\mathbf{F}^T$ is the left Cauchy Green strain tensor, and:

$$\delta_1 = \frac{2}{\sqrt{I_3}}\left(I_2\frac{\partial W}{\partial I_2} + I_3\frac{\partial W}{\partial I_3}\right); \quad \delta_2 = \frac{2}{\sqrt{I_3}}\frac{\partial W}{\partial I_1}; \quad \delta_3 = -2\sqrt{I_3}\frac{\partial W}{\partial I_2} \tag{8}$$

One can note that some authors used sometimes the eigenvalues λ_i^2 of $\mathbf{C}$ (which represent the main stretches) rather than the principal invariants I_i [6,23]. In this context, it has been reported in [31] that a special attention must be paid from a computational point of view to the special cases of double and triple coalescence.

2.2. Classical hyperelastic models

The energy function W can be obtained by a molecular or a phenomenological approach. Fig. 1 provides a non exhaustive list of some standard densities and their affiliation to one or other of the two categories, molecular or phenomenological. Treloar [32] has provided an overview of these two kinds of approaches and more recently, Marckmann and Verron [19] have given criteria to compare many popular models from the literature.

However, one often meets problems to fit well numerical results coming from the classical models with experimental data in the law deformation range [5,9] or in the large compressive range [24]. To overcome this problem, Flory and Erman [7] have separated the energy density into two parts:

$$W = W_a + W_c \tag{9}$$

where W_a is the affine part also called phantom energy which considers the release of the material chains while W_c represents the constraint part of the intertwining chains in the material matrix. The phantom energy, which is based on statistical consideration, involves the invariant I_1 while the constraint energy, which is a molecular one, depends on the eigenvalues λ_i^2 of $\mathbf{C}$ [33,34]:

$$W_c = \frac{1}{2} N k_B T \sum_{i=1}^{3} \left[B_i + D_i - \ln(1 + B_i) - \ln(1 + D_i) \right] \tag{10}$$

$$B_i = \kappa^2 \frac{\lambda_i^2 - 1}{(\lambda_i^2 + \kappa)^2}; \quad D_i = \frac{\lambda_i^2}{\kappa} B_i \tag{11}$$

where N, k_B, T and κ represent respectively the number of chains, the Boltzmann constant, the absolute temperature and the measure of strengths of the constraint.

From Eq. (10), Boyce and Arruda [35] improved the degree of correlation of their preliminary 8-chains model:

$$W = \mu\, n \left[\frac{\lambda_a \beta_a - \beta_{ao}}{\sqrt{n}} + \ln\left(\frac{\beta_a \sinh \beta_{ao}}{\beta_{ao} \sinh \beta_a} \right) \right] + \frac{1}{2} N k_B T \sum_{i=1}^{3} \left[B_i + D_i - \ln(1 + B_i) - \ln(1 + D_i) \right] \tag{12}$$

where $\lambda_a = \sqrt{\frac{I_1}{3}}$ represents the mean stretch of the material, sinh represents the hyperbolic sinus function, β_a is connected to the inverse of the Langevin function $\mathcal{L}^{-1}$ by $\beta_a = \mathcal{L}^{-1}(\frac{\lambda_a}{\sqrt{n}})$ and n is the number of chains per unit volume. The term $\beta_{a0} = \mathcal{L}^{-1}(\frac{1}{\sqrt{n}})$ is introduced to take into account the fact that W must be equal to zero for a material at rest. We finally recall that the Langevin function $\mathcal{L}$ is related to the hyperbolic cotangent function coth by:

$$\mathcal{L}(x) = \coth(x) - \frac{1}{x} \tag{13}$$

Kroon [2] also used the Arruda and Boyce 8-chain model by including a function of the second invariant I_2, to account for the constraint part of the energy density, and by incorporating an additional power form energy density to account for the surrounding polymer network:

$$W = \mu\, n \left[\frac{\lambda_a \beta_a - \beta_{ao}}{\sqrt{n}} + \ln\left(\frac{\beta_a \sinh \beta_{ao}}{\beta_{ao} \sinh \beta_a} \right) \right] + C_c \sqrt{\frac{I_2}{3}} + C_{na} (\lambda_{na} - 1)^{\alpha} \tag{14}$$

where C_c, C_{na} and α are additional parameters, λ_{na} represents the stretch associated with the additional compliance coming from the surrounding polymer network. λ_a and λ_{na} are linked by $\lambda_a \lambda_{na} = \sqrt{\frac{I_1}{3}}$.

The second term in Eq. (14) represents the interleaving energy of the chains of the Kroon model. Other authors have proposed an interleaving energy in a logarithmic form [3,5,10,21] or in a power form [11,22,36]:

$$W_c = K \ln\left(\frac{I_2}{3} \right) \tag{15}$$

$$W_c = K (I_2 - 3)^{\zeta} \quad \text{with } 0 < \zeta < 1 \tag{16}$$

Due to the power form of Eq. (16), it is noted that discontinuity occurs between a tensile and a compressive behavior if W_c is derivated with respect to I_2.

3. A new incompressible isotropic hyperelastic model

The goal of this section is to propose a new isotropic model which takes into account the behavior of the polymer chains contained in the elastomeric matrix as shown in Fig. 2.

During the deformation of a specimen (with an initial length noted L_0 and the current length noted L – see Fig. 2), the chains may act in three ways. The chains labelled by 1 on Fig. 2 have an affine deformation corresponding to the fact that the elongation of the chain is the same as that of the specimen. Their behavior can be represented by an affine energy density W_a. The chains labelled by 2 interleave other chains and can be modelled by a second energy density noted W_c. Finally, the chains labelled by 3 present an non-affine deformation illustrated on Fig. 2 (right) by a non-proportional elongation of the chain with respect to the current length L of the specimen. In Kroon [2], this behavior is embedded in a penalized term linking the macroscopic stretch to the stretch of the chain. In our model, we have completed W_a and W_c by a third term labeled W_{pid} (where the subscript *pid* stands for phenomenological integral density) which allows to balance the mismatch between model and data:

$$W = W_a + W_c + W_{pid} \tag{17}$$

This third density is one of the main original contributions of this paper and we will see later that it adopts a particular integral form. Because it completes efficiently the affine strain energy density W_a, one could argue that the density W_{pid} includes the effect of non-affine deformation. But this issue has to be more deeply investigated in order to be established beyond any doubt and the present paper is not focused on that point.

If we consider the special case of a uniaxial tension in direction X_1, the principal stretches reduce to:

$$\lambda_1 = \lambda; \quad \lambda_2 = \lambda_3 = \lambda^{-1/2} \tag{18}$$

and the tensile Cauchy stress can be easily deduced from Eqs. (7), (8) and (17):

$$\Sigma_1 = 2\left(\lambda^2 - \frac{1}{\lambda} \right) \left[\left(\frac{\partial W_a}{\partial I_1} + \frac{1}{\lambda} \frac{\partial W_a}{\partial I_2} \right) + \left(\frac{\partial W_c}{\partial I_1} + \frac{1}{\lambda} \frac{\partial W_c}{\partial I_2} \right) + \left(\frac{\partial W_{pid}}{\partial I_1} + \frac{1}{\lambda} \frac{\partial W_{pid}}{\partial I_2} \right) \right] \tag{19}$$

By using the eigenvalues of **B** (which are the same as that of **C**) instead of the principal invariants, Eq. (19) can be shortened to:

$$\Sigma_1 = \Sigma_{a1} + \Sigma_{c1} + \Sigma_{pid1} = \lambda \left(\frac{\partial W_a}{\partial \lambda} + \frac{\partial W_c}{\partial \lambda} + \frac{\partial W_{pid}}{\partial \lambda} \right) \tag{20}$$

The following is dedicated to a separated analysis of the affine part Σ_{a1}, of the constraint part Σ_{c1} and of the phenomenological integral part Σ_{pid1} of the Cauchy stress and to the determination of the corresponding energy densities W_a, W_c and W_{pid}.

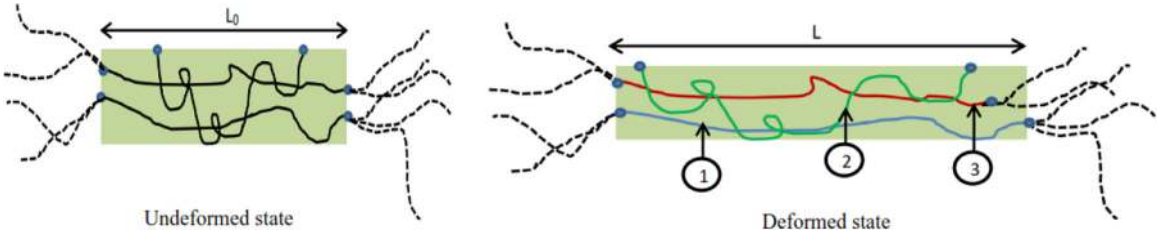

Fig. 2. Behavior of the polymer chains during the deformation.

3.1. Affine energy density

Following the work of Arruda and Boyce [1], we have adopted the 8-chains model described by the first term of Eq. (12):

$$W_a = \mu n\left[\frac{\lambda_a\beta_a - \beta_{ao}}{\sqrt{n}} + \ln\left(\frac{\beta_a \sinh\beta_{ao}}{\beta_{ao}\sinh\beta_a}\right)\right] \tag{21}$$

In the context of a uniaxial tensile loading, the combination of Eqs. (19) and (21) gives:

$$\Sigma_{a1} = \frac{\mu}{3}\left(\lambda^2 - \frac{1}{\lambda}\right)\frac{\sqrt{n}}{\lambda_a}\mathcal{L}^{-1}\left(\frac{\lambda_a}{\sqrt{n}}\right) \tag{22}$$

However, it is well known that the inverse of the Langevin function $\mathcal{L}^{-1}$, which appears in Eq. (22), cannot be expressed in an explicit form but can be either approximated by rational function [37–39] or by means of a Taylor expansion [40,41]. In this work, we decided to use a very recent and accurate approximation (with a maximum relative error lower than 0.05%) introduced by Nguessong et al. [25]:

$$\mathcal{L}^{-1}\left(\frac{\lambda_a}{\sqrt{n}}\right) \simeq \frac{\lambda_a}{\sqrt{n}}\frac{3 - \left(\frac{\lambda_a}{\sqrt{n}}\right)^2}{1 - \left(\frac{\lambda_a}{\sqrt{n}}\right)^2} - 0.488\left(\frac{\lambda_a}{\sqrt{n}}\right)^{3.243} + 3.311\left(\frac{\lambda_a}{\sqrt{n}}\right)^{4.789}\left(\frac{\lambda_a}{\sqrt{n}} - 0.76\right)\left(\frac{\lambda_a}{\sqrt{n}} - 1\right) \tag{23}$$

3.2. Interleaving energy density

We have previously mentioned two options to model the behavior of the intertwining molecular chains by an interleaving energy density (Eqs. (10) or (15)). To select the best one, the advantages and drawbacks of both of them are discussed in this section. We first deduce from Eq. (20) the Cauchy stress Σ_{c1} related to the molecular energy density (10):

$$\Sigma_{c1} = \lambda\frac{\partial W_c}{\partial\lambda} = \frac{Nk_BT}{2}\lambda\left[\frac{dB_1}{d\lambda}\left(\frac{B_1}{1+B_1}\right) + \frac{dB_2}{d\lambda}\left(\frac{B_2}{1+B_2}\right) + \frac{dB_3}{d\lambda}\left(\frac{B_3}{1+B_3}\right) + \frac{dD_1}{d\lambda}\left(\frac{D_1}{1+D_1}\right) + \frac{dD_2}{d\lambda}\left(\frac{D_2}{1+D_2}\right) + \frac{dD_3}{d\lambda}\left(\frac{D_3}{1+D_3}\right)\right] \tag{24}$$

with:

$$B_1 = \kappa^2\frac{\lambda^2 - 1}{\left(\lambda^2+\kappa\right)^2}, \quad D_1 = \frac{\lambda^2}{\kappa}B_1, \quad B_2 = B_3 = \kappa^2\frac{\frac{1}{\lambda} - 1}{\left(\frac{1}{\lambda}+\kappa\right)^2}, \quad D_2 = D_3 = \frac{B_2}{\lambda\kappa} \tag{25}$$

$$\frac{dB_1}{d\lambda} = \kappa^2\frac{2\lambda\left(\kappa + 2 - \lambda^2\right)}{\left(\lambda^2+\kappa\right)^3}, \quad \frac{dD_1}{d\lambda} = \frac{\lambda}{\kappa}\left(2B_1 + \lambda\frac{dB_1}{d\lambda}\right)$$

$$\frac{dB_2}{d\lambda} = \frac{dB_3}{d\lambda} = \kappa^2\frac{\frac{1}{\lambda} - \kappa - 2}{\lambda^2\left(\frac{1}{\lambda}+\kappa\right)^3}, \quad \frac{dD_2}{d\lambda} = \frac{dD_3}{d\lambda} = \frac{1}{\lambda\kappa}\left(\frac{dB_2}{d\lambda} - \frac{B_2}{\lambda}\right) \tag{26}$$

The Cauchy stress of the interleaving chains part related to the phenomenological energy (15) is obtained in the same manner:

$$\Sigma_{c1} = \lambda\frac{\partial W_c}{\partial\lambda} = 2\left(\lambda - \frac{1}{\lambda^2}\right)\frac{K}{I_2} \tag{27}$$

The stress components Σ_{c1} described by Eqs. (24) and (27) are plotted on Fig. 3. The corresponding curves present a similar trend with an increasing stress versus the elongation λ. It is also noted an asymptotic behavior when λ tends towards infinity. It can be easily demonstrated that the asymptotic value is Nk_BT for the molecular model while it is equal to K for the phenomenological model. Fig. 3 therefore reveals that there are no physical argument for choosing one model over another. However, it is noted, by comparing Eqs. (24)–(26) on the one hand to Eq. (27) on the other hand, that the phenomenological model provides a simpler algebraic expression than the molecular model. In view of a finite element implementation, we have therefore decided to include the phenomenological density given by Eq. (15) in our model.

3.3. Integral energy density

In the two previous sections, we have opted for the affine 8-chains energy and for the interleaving energy defined by Eq. (15). In this paragraph, we will determine step by step the expression of the phenomenological integral energy density. To have an intuition for building this density, we first focus on the particular case of a uniaxial tension-compression loading, based on the

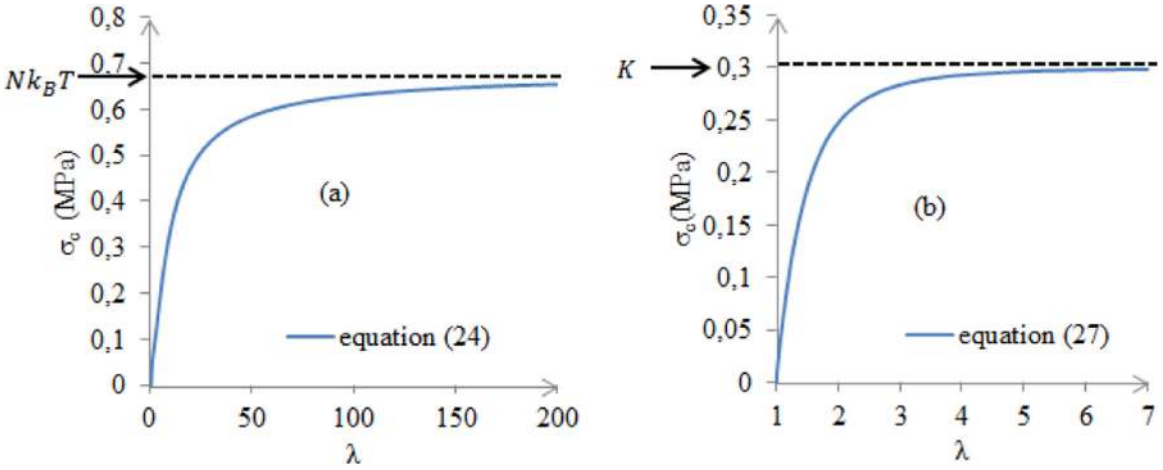

Fig. 3. Behavior of the stress component Σ_{c1}. The rheological parameters are Nk_BT = 0.68 MPa, κ = 0.55, K = 0.3 MPa [10,35].

experimental data of Yeoh and Fleming [27]. Then we will go to the general case.

3.3.1. Uniaxial tension-compression case

We start from the general expression of the Cauchy stress (Eq. (20)) where we have reported the contributions of the 8-chains model (Eq. (22)) and of the interleaving energy proposed by Gent and Thomas (Eq. (27)):

$$\Sigma_1 = 2\left(\lambda^2 - \frac{1}{\lambda}\right)\left[\frac{\mu}{6}\frac{\sqrt{n}}{\lambda_a}\mathcal{L}^{-1}\left(\frac{\lambda_a}{\sqrt{n}}\right) + \frac{K}{\lambda I_2}\right] + \Sigma_{pid1} \tag{28}$$

To highlight the fundamental influence of the phenomenological integral stress Σ_{pid1} (the last term in Eq. (28)), we set it first to zero and we will prove that the two other terms, namely Σ_{a1} and Σ_{c1}, are inefficient to well predict the experimental data of the uniaxial and compression tests performed by Yeoh and Fleming on natural vulcanized rubber [27]. To perform the comparison between the theoretical and the experimental data, we have chosen the Mooney plot because it is a very sensitive curve for the validation of isotropic hyperelastic models [10,13,42,43].

Eq. (28) (where we recall that we have set Σ_{pid1} temporarily to zero) can be written in the Mooney form [4] by introducing the reduced stress Φ:

$$\Phi\left(\frac{1}{\lambda}\right) = \frac{\Sigma_1}{\lambda^2 - \frac{1}{\lambda}} = 2\left[\frac{\mu}{6}\frac{\sqrt{n}}{\lambda_a}\mathcal{L}^{-1}\left(\frac{\lambda_a}{\sqrt{n}}\right) + \frac{K}{\lambda I_2}\right] \tag{29}$$

The identification of the rheological parameters μ, n and K were performed by minimizing the quadratic difference between Φ and the experimental reduced stress Φ_{exp}:

$$\min_{\mu,n,K} obj = \sum\left[\frac{\left(\Phi_{exp} - \Phi\right)^2}{\Phi_{exp}^2}\right] \tag{30}$$

where the sum in Eq. (30) is performed over all the tested values of λ. The identified values of μ, n and K are reported in the caption of Fig. 4. As announced, this figure shows that the reduced stress defined by Eq. (29) presents a poor prediction for the large compressive range (i.e. $\frac{1}{\lambda} > 1.5$).

To overcome this difficulty, we have used the in-stages-approach developed by Beda and Chevalier [44] to analyse the behavior of the residual $\Theta(\frac{1}{\lambda})$ defined below:

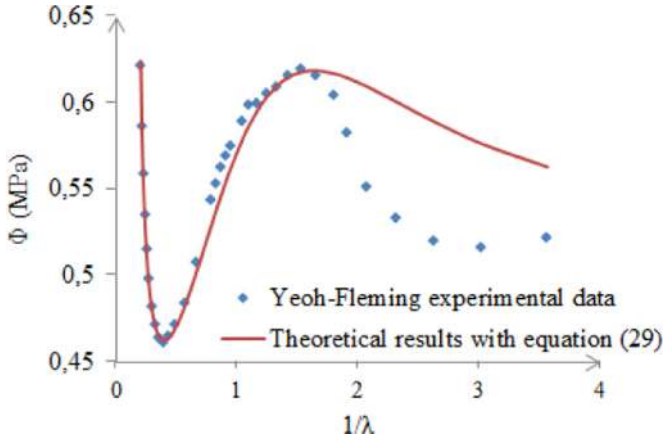

Fig. 4. Reduced stress prediction from Eq. (29) with $\mu = 0.3805$ MPa, n = 15.13 and $K = 0.26$ MPa.

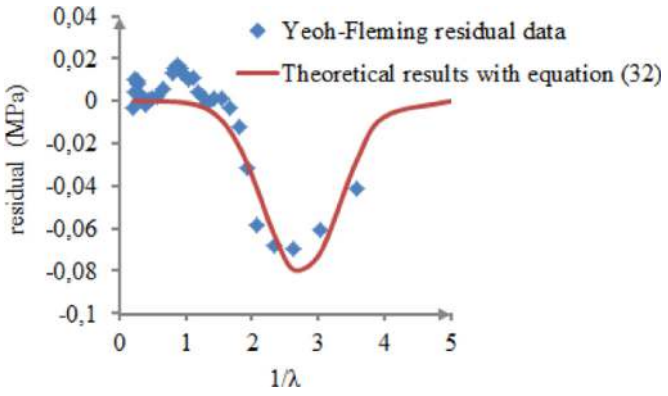

Fig. 5. Residual prediction from the phenomenological integral reduced stress (Eq. (32)) with $\eta = 0.081$ MPa, $\zeta = 2.741$ and $\xi = 0.813$.

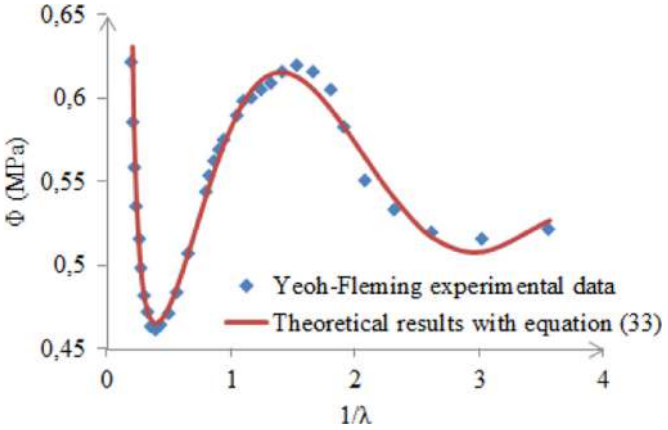

Fig. 6. Comparison of Yeoh–Fleming experimental data with the reduced stress of Eq. (33).

$$\Theta\left(\frac{1}{\lambda}\right) = \Phi_{exp} - \Phi = \frac{\Sigma_{exp}}{\lambda_{exp}^2 - \frac{1}{\lambda_{exp}}} - 2\left[\frac{\mu}{6}\frac{\sqrt{n}}{\lambda_a}\mathcal{L}^{-1}\left(\frac{\lambda_a}{\sqrt{n}}\right) + \frac{K}{\lambda I_2}\right] \tag{31}$$

where Σ_{exp} and λ_{exp} represent respectively the experimental stress and the experimental elongation.

One can observe on Fig. 5 that this residual Θ presents a shape close to the one of a Gaussian function, at least in the left part and in the vicinity of the minimum of this Gaussian function which correspond to the locations of the experimental data points. This observation leads us to adopt a Gaussian function Φ_{pid} to approximate the behavior of Θ:

$$\Theta\left(\frac{1}{\lambda}\right) \approx \Phi_{pid}\left(\frac{1}{\lambda}\right) = -\eta\exp\left[-\left(\frac{\frac{1}{\lambda} - \zeta}{\xi}\right)^2\right] \tag{32}$$

where η, ζ and ξ represent respectively the maximum amplitude, the abscissa of the maximum and the square root of twice the

Table 1
Parameters of Eq. (33) identified with the Yeoh–Fleming data [27].

Parameters	μ (MPa)	n (−)	K (MPa)	η (MPa)	ζ (−)	ξ (−)
Values	0.379	14.9	0.295	0.096	2.708	1.132

variance of Φ_{pid}. These coefficients were identified through a least square optimization of the difference between Θ and Φ_{pid} (see the caption of Fig. 5).

Using the improvement provided by Eq. (32) to modify Eq. (29) gives:

$$\Phi\left(\frac{1}{\lambda}\right) = \frac{\Sigma_1}{\lambda^2 - \frac{1}{\lambda}} = 2\left[\frac{\mu}{6}\frac{\sqrt{n}}{\lambda_a}\mathcal{L}^{-1}\left(\frac{\lambda_a}{\sqrt{n}}\right) + \frac{K}{\lambda I_2}\right] - \eta \exp\left[-\left(\frac{\frac{1}{\lambda} - \zeta}{\xi}\right)^2\right] \tag{33}$$

The six rheological parameters μ, n, K, η, ζ and ξ embedded in Eq. (33) were identified by using the Levenberg–Marquardt algorithm (Table 1).

By comparing Figs. 4 and 6, it is obvious that the inclusion of a Gaussian contribution through Eq. (32) provides a better approximation of the experimental data than the one provided by Eq. (29).

A new behavior law can be deduced from Eq. (33) but it only holds for a uniaxial tensile or compressive loading:

$$\Sigma_1 = 2\left(\lambda^2 - \frac{1}{\lambda}\right)\left\{\frac{\mu}{6}\frac{\sqrt{n}}{\lambda_c}\mathcal{L}^{-1}\left(\frac{\lambda_a}{\sqrt{n}}\right) + \frac{K}{\lambda I_2} - \frac{\eta}{2}\exp\left[-\left(\frac{\frac{1}{\lambda} - \zeta}{\xi}\right)^2\right]\right\} \tag{34}$$

Considering both Eqs. (28) and (34) leads to the following phenomenological constraint part Σ_{pid1}:

$$\Sigma_{pid1} = -\eta\left(\lambda^2 - \frac{1}{\lambda}\right)\exp\left[-\left(\frac{\frac{1}{\lambda} - \zeta}{\xi}\right)^2\right] \tag{35}$$

At this stage, two questions arise:

1. What kind of energy density W_{pid} can be associated to the phenomenological constraint part Σ_{pid1} introduced by Eq. (35)?
2. If the first question can be addressed, how to extend to the general case the energy density W_{pid} which has been determined in a special uniaxial case?

The answer to the first question is quite simple. From Eqs. (20) and (35), the phenomenological integral constraint part Σ_{pid1} can be related to a phenomenological integral energy density W_{pid} by:

$$\Sigma_{pid1} = \lambda\frac{\partial W_{pid}}{\partial\lambda} \Rightarrow W_{pid} = -\eta\int_1^\lambda\left(s - \frac{1}{s^2}\right)\exp\left[-\left(\frac{\frac{1}{s} - \zeta}{\xi}\right)^2\right]ds \tag{36}$$

One can note that the energy density given by Eq. (36) adopts an integral form. It can not a priori be integrated but that causes no specific problem because we only need to derive W_{pid} to obtain the stress tensor.

The answer to the second question, which is more complex, is studied in the next section.

3.3.2. General case

In the most general case, W_{pid} depends on the three invariants of the left Cauchy–Green tensor $\mathbf{B}$:

$$W_{pid}(\mathbf{B}) = W_{pid}\left[I_1(\mathbf{B}), I_2(\mathbf{B}), I_3(\mathbf{B})\right] \tag{37}$$

Reporting (37) in Eqs. (7)–(8) with $I_3 = 1$ gives:

$$\boldsymbol{\Sigma}_{pid} = 2\left[\frac{\partial W_{pid}}{\partial I_1}\mathbf{B} - \frac{\partial W_{pid}}{\partial I_2}\mathbf{B}^{-1}\right] - p\mathbf{I} \tag{38}$$

where p is a Lagrange multiplier which is classically introduced to account for the incompressibility condition.

We next consider the observation made by Kroon [2] and assume that W_{pid} only depends on I_1. In the uniaxial case, the general formula (38) thus reduces to:

$$\boldsymbol{\Sigma}_{pid} = \begin{pmatrix} 2\lambda^2\frac{dW_{pid}}{dI_1} - p & 0 & 0 \\ 0 & \frac{2}{\lambda}\frac{dW_{pid}}{dI_1} - p & 0 \\ 0 & 0 & \frac{2}{\lambda}\frac{dW_{pid}}{dI_1} - p \end{pmatrix} \tag{39}$$

By using the free boundary conditions $\Sigma_{pid2} = \Sigma_{pid3} = 0$ (where Σ_{pid1}, Σ_{pid2} and Σ_{pid3} represent the diagonal terms of $\boldsymbol{\Sigma}_{pid}$), it is easy to calculate p and next to report the result to calculate the tensile stress Σ_{pid1}:

$$\Sigma_{pid1} = 2\left(\lambda^2 - \frac{1}{\lambda}\right)\frac{dW_{pid}}{dI_1} \tag{40}$$

The comparison of Eqs. (35) and (40) leads to:

$$\frac{dW_{pid}}{dI_1} = -\frac{\eta}{2}\exp\left[-\left(\frac{\frac{1}{\lambda} - \zeta}{\xi}\right)^2\right] \tag{41}$$

In order to integrate Eq. (41), we need to have the same variable on both sides of the equation. We therefore need to establish a link between I_1 and λ. This link is easily obtained from Eq. (18):

$$I_1 = \lambda^2 + \frac{2}{\lambda} = g(\lambda) \tag{42}$$

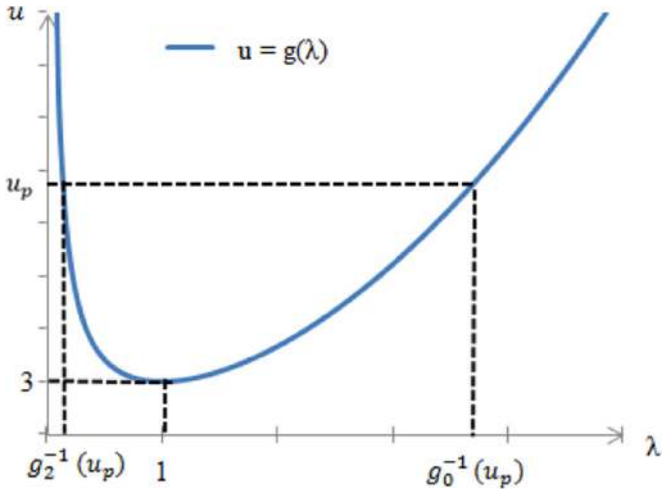

Fig. 7. Behavior of $g(\lambda)$ (Eq. (42)).

By introducing the inverse g^{-1} of the function g defined by Eq. (42), we obtain from Eq. (41):

$$W_{pid} = -\frac{\eta}{2}\int_3^{I_1} \exp\left[-\left(\frac{\left(g^{-1}(u)\right)^{-1}-\zeta}{\xi}\right)^2\right] du \tag{43}$$

We have thus succeeded to calculate W_{pid} but Eq. (43) is fully determined if, and only if, the reciprocal function $\lambda = g^{-1}(u)$ is known. Unfortunately, it can be seen on Fig. 7 that the function g is not bijective on $\mathbb{R}^+$ (which is the interesting set because λ is a physical positive number). But g can be considered as a bijective function if we restrict the study on the intervals $]0, 1]$ or $[1, +\infty[$.

It then exists a unique solution on each interval: $g_2^{-1}(u_p) \in]0, 1]$ which represents a compressive solution and $g_0^{-1}(u_p) \in [1, +\infty[$ representing a tensile solution. To calculate these two solutions, we remark that Eq. (42) leads to a cubic polynomial equation:

$$\left[g_k^{-1}(u)\right]^3 - u\left[g_k^{-1}(u)\right] + 2 = 0 \quad \text{with } u \geq 3 \tag{44}$$

This equation can be solved by means of the Cardano's formula:

$$g_k^{-1}(u) = 2\sqrt{\frac{u}{3}}\cos\left[\frac{1}{3}\arccos\left(-\sqrt{\frac{27}{u^3}}\right) + \frac{2k\pi}{3}\right] \quad k = 0, 1, 2 \tag{45}$$

It has been demonstrated by Nguessong [24] that the case of $k=0$ corresponds to the tensile solution, the case $k=1$ to a negative unphysical solution and the case $k=2$ to the compressive solution. We have now just to decide what is the best choice between $g_0^{-1}(u)$ and $g_2^{-1}(u)$ to be reported in Eq. (43). Since the phenomenological integral energy density was built to correct the prediction error in the compressive range, we logically decided to select $g_2^{-1}(u)$:

$$W_{pid} = -\frac{\eta}{2}\int_3^{I_1} \exp\left[-\left(\frac{\left(g_2^{-1}(u)\right)^{-1}-\zeta}{\xi}\right)^2\right] du \tag{46}$$

To evaluate the phenomenological integral density W_{pid}, we perform the following change of variable:

$$x = H(u) = \frac{\left(g_2^{-1}(u)\right)^{-1}-\zeta}{\xi} \Rightarrow H(I_1) = \frac{\left(g_2^{-1}(I_1)\right)^{-1}-\zeta}{\xi}; \quad H(3) = \frac{1-\zeta}{\xi} \tag{47}$$

The differential term du is related to dx from Eqs. (47) and (42):

$$u = g_2\left[(\xi x+\zeta)^{-1}\right] = (\xi x+\zeta)^{-2} + 2\left(\xi x+\zeta\right) \Rightarrow du = 2\xi\left[1-\frac{1}{(\xi x+\zeta)^3}\right]dx \tag{48}$$

Using Eqs. (46), (47) and (48) yields to:

$$W_{pid} = -\eta\xi\left\{\int_{H(3)}^{H(I_1)} \exp(-x^2)\,dx - \int_{H(3)}^{H(I_1)} \frac{\exp(-x^2)}{(\xi x+\zeta)^3}\,dx\right\} \tag{49}$$

The first term of Eq. (49) can also be written:

$$\int_{H(3)}^{H(I_1)} \exp(-x^2)\,dx = \frac{\sqrt{\pi}}{2}\left[Erf\left(H(I_1)\right) - Erf\left(H(3)\right)\right] \tag{50}$$

where the error function Erf is defined by:

$$Erf(u) = \frac{2}{\sqrt{\pi}}\int_0^u \exp\left[-x^2\right]dx = \frac{2}{\sqrt{\pi}}\sum_{n=0}^{+\infty}\frac{(-1)^n u^{2n+1}}{n!(2n+1)} \tag{51}$$

The second term of Eq. (49) is calculated by the integration of a Taylor expansion of the rational expression $\frac{\exp(-x^2)}{(\xi x+\zeta)^3}$:

$$\frac{\exp\left(-x^2\right)}{(\xi x+\zeta)^3} = \sum_{n=0}^{+\infty} C_n x^n \tag{52}$$

where

$$C_n = \frac{(-1)^n}{2\zeta^3}\sum_{k=0}^{ent\left(\frac{n}{2}\right)}(-1)^k\frac{(n-2k+2)(n-2k+1)}{k!}\left(\frac{\xi}{\zeta}\right)^{n-2k} \tag{53}$$

and *ent* represents the whole part of a real number.

Reporting the Taylor expansion (52) into the second term of Eq. (49) gives:

$$\int_{H(3)}^{H(I_1)} \frac{\exp\left(-x^2\right)}{(\xi x+\zeta)^3}\,dx = \frac{\sqrt{\pi}}{2}\left[Erf3\left(H(I_1)\right) - Erf3\left(H(3)\right)\right] \tag{54}$$

where the $Erf3$ function is defined by:

$$Erf3(u) = \frac{2}{\sqrt{\pi}}\int_0^u \frac{\exp\left(-x^2\right)}{(\xi x+\zeta)^3}\,dx = \frac{2}{\sqrt{\pi}}\sum_{n=0}^{+\infty}\frac{C_n}{n+1}u^{n+1} \tag{55}$$

The energy density W_{pid} can thus be expressed only in terms of error functions by combining Eqs. (49), (50) and (54):

$$W_{pid} = -\eta\xi\frac{\sqrt{\pi}}{2}\left\{Erf\left(H(I_1)\right) - Erf\left(H(3)\right) - Erf3\left(H(I_1)\right) + Erf3\left(H(3)\right)\right\} \tag{56}$$

Or, equivalently, by using the Taylor expansions (51) and (55) and Eq. (47):

$$W_{pid} = -\eta\xi\sum_{n=0}^{+\infty}\frac{(-1)^n\left[\left(\left(g_2^{-1}(I_1)\right)^{-1}-\zeta\right)^{2n+1} - (1-\zeta)^{2n+1}\right]}{n!(2n+1)\xi^{2n+1}} - \frac{C_n\left[\left(\left(g_2^{-1}(I_1)\right)^{-1}-\zeta\right)^{n+1} - (1-\zeta)^{n+1}\right]}{(n+1)\xi^{n+1}} \tag{57}$$

Eq. (57) shows that it is not easy to guess for a replacement of the non-closed form representation (46) of W_{pid} by a finite number of polynomials. Additionally, the convergence of the Taylor expansion introduced by Eq. (52) and related to the fractional term of Eq. (49) depends on the value of x. The second term in Eq. (57) can therefore possibly provide a rather poor approximation of the integral introduced by Eq. (54). However, keeping the strain energy density in the integral form described by Eq. (46) is not a drawback because we can deduce from it an extremely simple relation between the strain and the stress fields. Deriving the integral will actually force the integral to disappear and a closed form behavior law will be obtained.

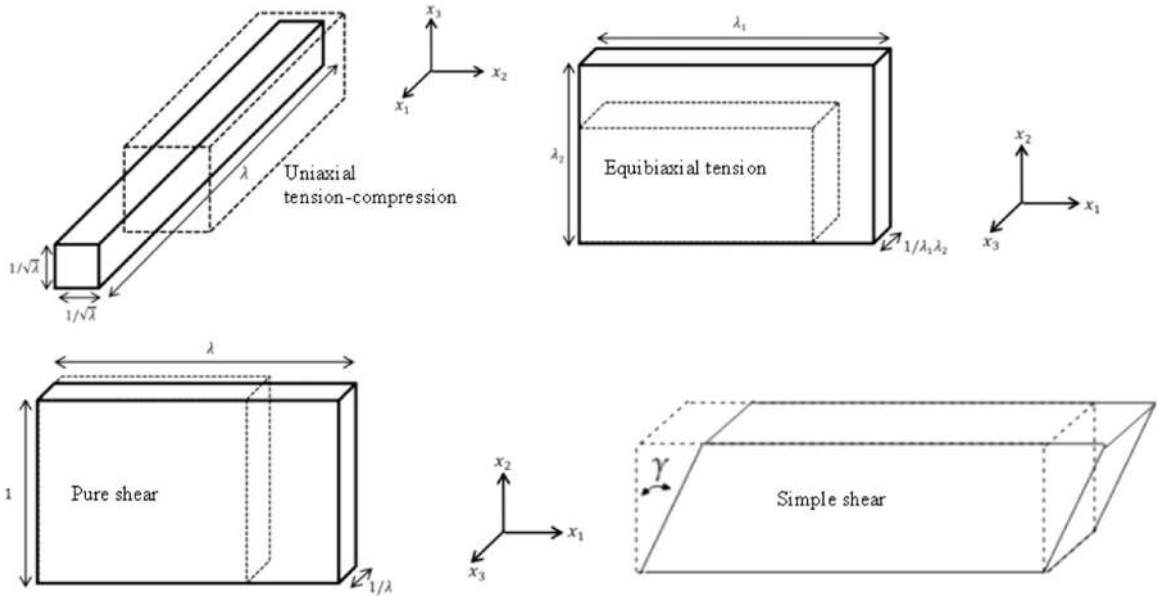

Fig. 8. Different types of loading.

Table 2
Identified rheological parameters of the models - experimental data from Treloar [26].

Parameters	μ (MPa)	n (−)	J_m (−)	K (MPa)	η (MPa)	ζ (−)	ξ (−)
Arruda–Boyce	0.31	26.83	–	–	–	–	–
Pucci–Saccomandi	0.262	–	84.57	0.295	–	–	–
HIA	0.3579	27.66	–	0.1266	0.1011	0.319	0.327

Table 3
Identified rheological parameters of the models - experimental data from Arruda and Boyce [1].

Parameters	μ (MPa)	n (−)	J_m (−)	K (MPa)	η (MPa)	ζ (−)	ξ (−)
Arruda–Boyce	0.45	12.17	–	–	–	–	–
Pucci-Saccomandi	0.441	–	36.509	0.029	–	–	–
HIA	0.117	9.03	–	1.284	0.717	1.554	2.116

Table 4
Identified rheological parameters of the models - experimental data from Yeoh and Fleming [27].

Parameters	μ (MPa)	n (−)	J_m (−)	K (MPa)
Arruda–Boyce	0.494	37	–	–
Pucci–Saccomandi	0.39	–	57	0.265

All the observations made in this section have led us to propose a new HIA (Hybrid Integral Approach) energy density which combines the 8-chains energy density to model the affine strain of polymeric chains (Eq. (21)), a phenomenological energy density to model the interleaving constraint chains (Eq. (15)) and the phenomenological integral density to balance the mismatch between model and data (Eq. (46)):

$$W = \mu\, n\left[\frac{\lambda_a\beta_a - \beta_{ao}}{\sqrt{n}} + \ln\left(\frac{\beta_a \sinh\beta_{ao}}{\beta_{ao}\sinh\beta_a}\right)\right] - \frac{\eta}{2}\int_3^{I_1} \exp\left[-\left(\frac{\left(g_2^{-1}(u)\right)^{-1} - \zeta}{\xi}\right)^2\right] du + K\ln\left(\frac{I_2}{3}\right) \tag{58}$$

4. Experimental data analysis and discussion

We study in this section the capability of the new HIA model defined by the strain energy density (58) to predict the behavior of

Table 5
Identified rheological parameters of the models - experimental data from Nunes and Moreira [28].

Parameters	μ (MPa)	n (−)	J_m (−)	K (MPa)	η (MPa)	ζ (−)	ξ (−)
Arruda–Boyce	0.37	46.51	–	–	–	–	–
Pucci–Saccomandi	0.252	–	139.53	0.473	–	–	–
HIA	0.26	46.5	–	0.444	0.734	0.378	0.272

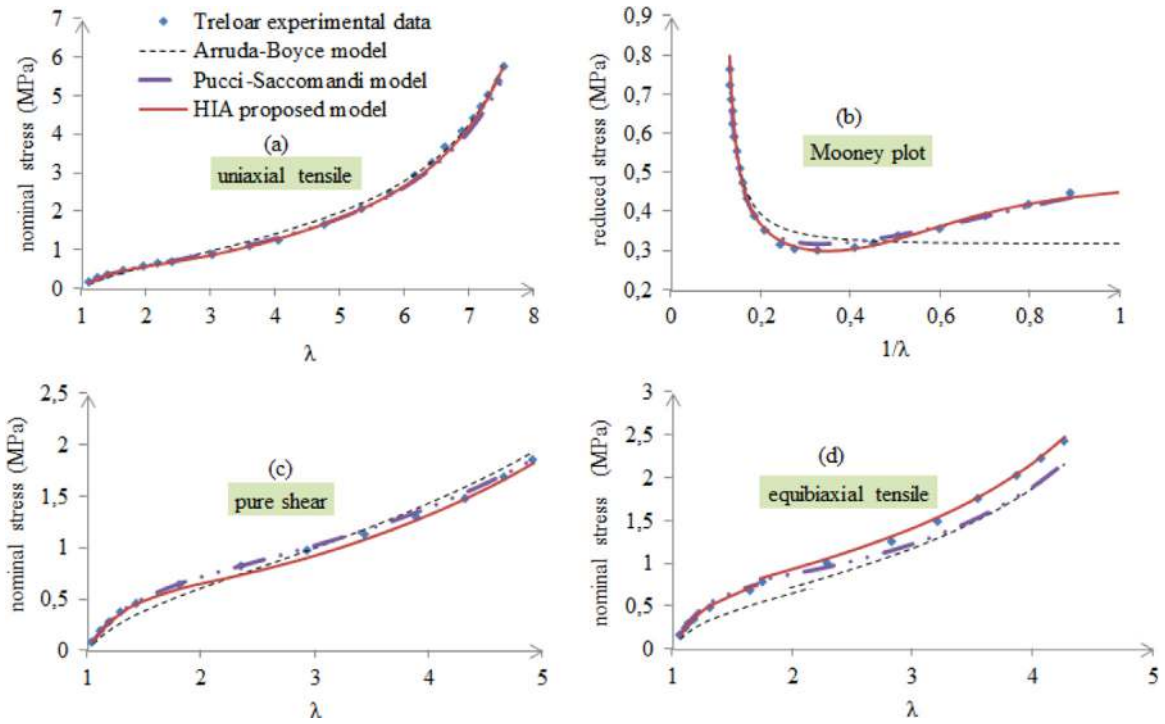

Fig. 9. Predictions of Arruda–Boyce model, Pucci–Saccomandi model and HIA proposed model compared to Treloar experimental data.

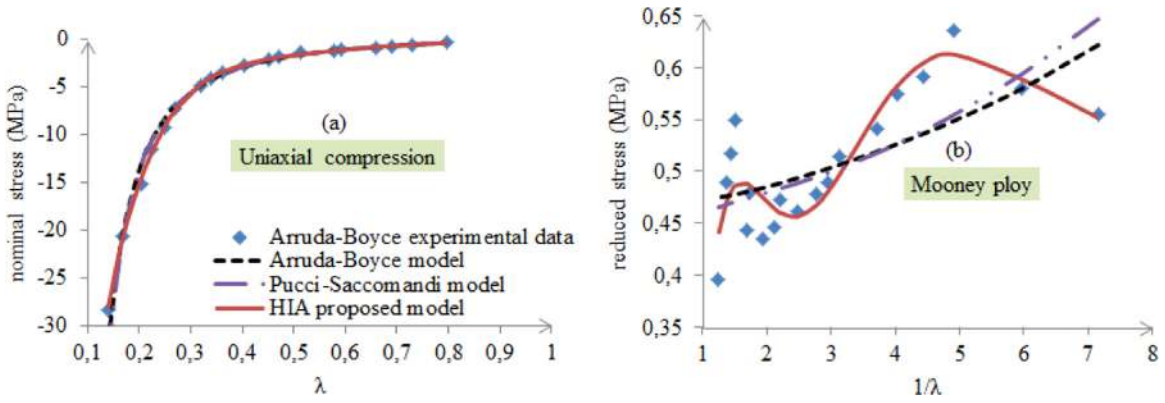

Fig. 10. Predictions of Arruda-Boyce model, Pucci–Saccomandi model and HIA proposed model compared to Arruda–Boyce experimental data.

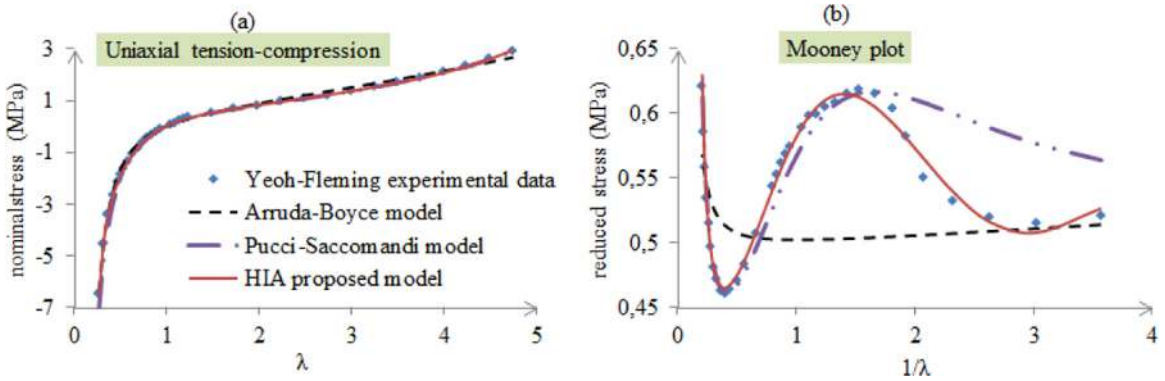

Fig. 11. Predictions of Arruda-Boyce model, Pucci–Saccomandi model and HIA proposed model compared to Yeoh-Fleming experimental data.

hyperelastic materials in the case of uniaxial and equibiaxial tension, uniaxial compression and pure and simple shear loading (Fig. 8). The study is made with experimental data extracted from [1,26–28]. Each data set corresponds to a different rubber material.

The performance of the HIA model is also compared to the 8-chains model of Arruda–Boyce and to the phenomenological model of Pucci–Saccomandi (also known as the Gent–Gent model) [21] given by:

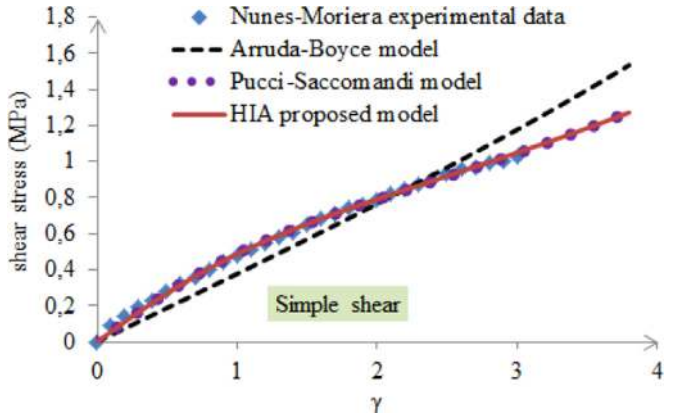

Fig. 12. Predictions of Arruda–Boyce model, Pucci–Saccomandi model and HIA proposed model compared to Nunes–Moriera experimental data.

$$W = -\frac{\mu}{2} J_m \ln\left(1 - \frac{I_1 - 3}{J_m}\right) + K \ln\left(\frac{I_2}{3}\right) \tag{59}$$

The rheological parameters of the three models were calculated with the Levenberg–Marquardt algorithm. The identified values are reported for each material in Tables 2–5.

4.1. Comparison with the treloar data

Treloar [26] performed testing on a vulcanized natural rubber under conditions of uniaxial and equibiaxial tension and pure shear loading.

In Fig. 9(a), one remarks that all the three models present a very good accuracy with the uniaxial tensile data, which is quite logical since the rheological parameters were identified from this test data. However, the Mooney plots (Fig. 9(b)) highlight differences that were not visible before. We observe in particular that the Arruda–Boyce model is excellent for final stiffening (very large deformations with: $0 < 1/\lambda < 0.3$) but clearly diverges for the moderate deformations ($1/\lambda > 0.3$). We can also observe a slight difficulty of prediction of the Pucci–Saccomandi model around the minimum ($1/\lambda = 0.3$). On the opposite to these two models, the HIA proposed model provides an excellent agreement.

In the case of pure shear loading (Fig. 9(c)), all the three models give very satisfactory prediction.

In the case of the equibiaxial tensile test (Fig. 9(d)), the general trends of the curves are well described by the Arruda–Boyce and the Pucci–Saccomandi models while the HIA proposed model agrees perfectly with the test data.

The HIA model is therefore not only able to fit well uniaxial data (Figs. 9a and b) but also provides excellent predictions with other types of loading (pure shear and equibiaxial tensile loading, Figs. 9c and d), by using the previously fitted material parameters.

4.2. Comparison with the Arruda–Boyce data

Arruda and Boyce [1] have performed a uniaxial compressive test on a silicone rubber.

Logically, the three models give an excellent prediction of the uniaxial compression test data (Fig. 10(a)), since the rheological parameters were identified on the basis of this test. In contrast, the Mooney plots (Fig. 10 (b)) show a great disparity for the models prediction except the HIA proposed model which gives a satisfactory description of the general trends of the curve.

4.3. Comparison with the Yeoh–Fleming data

Yeoh and Fleming [27] have performed a tension-compression test on a rubber vulcanized by sulfur and accelerator (N-Cyclohexyl-2-benzothiazolesulfenamide).

It is observed in Fig. 11(a) that each model presents a fair agreement with the experimental data. This result was again awaited because the identification of the rheological parameters was performed with the experimental data coming from the traction-compression test. However, if the comparison is performed in terms of the Mooney plot (Fig. 11(b)), the HIA proposed model obviously shows a higher accuracy than the Arruda–Boyce and the Pucci–Saccomandi models, particularly in the medium and high ranges of variation of $1/\lambda$.

4.4. Comparison with the Nunes–Moriera data

Nunes and Moreira [28] have performed a simple shear test on a silane modified polymer (Flextec FT 101).

Fig. 12 shows a very good accuracy of the Pucci–Saccomandi model and HIA proposed model with a relative quadratic error of $1.67 \cdot 10^{-4}$ for the first one and $1.57 \cdot 10^{-4}$ for the second one. It is noted, however, that the Arruda–Boyce constitutive law presents in this case a more approximative prediction of the test data than the two other models.

5. Conclusion

We have proposed in this paper a new approach (named HIA: Hybrid Integral Approach) to model the incompressible isotropic hyperelastic behavior of rubber-like materials. This model is based on the molecular 8-chain density introduced by Arruda and Boyce, includes a phenomenological logarithmic-form interleaving energy and offers an original phenomenological integral energy. The model is thus splitted in three different strain energy densities and takes advantage of both molecular and phenomenological approaches. It offers an excellent capability to predict the reduced stress of the Mooney plot thanks to the introduction of the original integral contribution. We have demonstrated that this model is able to well predict the stress-stretch response of different rubber materials [1,26–28]. This ability to reproduce experimental data was observed under various loading conditions (uniaxial and equibiaxial tension, uniaxial compression, pure and simple shear). However, it must be underlined that the high number of material parameters (6 in total) that are required to obtain a good agreement with the experimental results is the price we have to pay for outperforming the standard models of the literature. Compared for example to the Arruda–Boyce and to the Pucci–Saccomandi models, we must respectively triple and double the number of material parameters. The good performance of the proposed model has therefore to be balanced by the number of related material parameters, even if a number of six rheological parameters still remains a reasonable number. The good predictive abilities together with the numerically efficient structure of the model make it suitable for implementation in a finite element context.

This implementation in a University finite element software (calculation of second and fourth order tensors as the stiffness tangent matrix, application of the total Lagrangian approach, and use of the Newton–Raphson algorithm to solve the non-linear problem) will be developed in a following paper (part 2). This paper will also include numerous numerical applications involving contact and impact problems between deformable hyperelastic bodies.

Acknowledgment

This paper presents part of the work of the Ph.D. of Alain Nguessong Nkenfack defended on the 1st of April, 2015. This Ph.D. was carried out in close partnership between the University of Ngaoundéré (Cameroon) and the University of Technology of Belfort-Montbéliard (France). We gratefully acknowledge the financial support of the French embassy of France in Cameroon for the stays in France of the Ph.D. student. This work is also supported by the National Natural Science Foundation of China (Grant no. 11372260) for the stay in China of Z.-Q. Feng.

References

[1] E. Arruda, M. Boyce, A three-dimensional constitutive model for the large stretch behavior of rubber elastic materials, J. Mech. Phys. Solids 41 (1993) 389–412.
[2] M. Kroon, An 8-chain model for rubber-like materials accounting for non-affine chain deformations and topological constraints, J. Elast. 102 (2011) 99–116.
[3] A.N. Gent, A.G. Thomas, Forms for the stored (strain) energy function for vulcanized rubber, J. Polym. Sci. 28 (1958) 625–637.
[4] M. Mooney, A theory of large elastic deformation, J. Appl. Phys. 11 (1940) 582–596.
[5] L.J. Hart Smith. Elasticity parameter for finite deformations of rubber-like materials. Z. Angew. Math. Phys. 17 (1967) 608–626.
[6] R.W. Ogden, Large deformation isotropic elasticity: on the correlation of theory and experiment for incompressible rubber-like solids, Proc. – Rubber Soc. 326 (1972) 565–584.
[7] P.J. Flory, B. Erman, Theory of elasticity of polymer networks, Macromolecules 15 (1982) 800–806.
[8] O.H. Yeoh, Characterization of elastic properties of carbon-black-filled rubber vulcanizates, Rubber Chem. Technol. 63 (1990) 792–805.
[9] J. Lambert-Diani, C. Rey, New phenomenological behavior laws for rubbers and thermoplastic elastomers, Eur. J. Mech. A/Solids 18 (1999) 1027–1043.
[10] T. Beda, Modeling hyperelastic behavior of rubber: a novel invariant-based and a review of constitutive models, J. Polym. Sci.: Part B: Polym. Phys. 45 (2007) 1713–1732.
[11] M.M. Carroll, A strain energy function for vulcanized rubbers, J. Elast. 103 (2011) 173–187.
[12] J.D. Davidson, N.C. Goulbourne, A non-affine network model for elastomers undergoing finite deformations, J. Mech. Phys. Solids 61 (2013) 1784–1797.
[13] Zhu-Ping Huang, A novel constitutive formulation for rubber-like materials in thermoelasticity, J. Appl. Mech. 81 (2014) 1–8.
[14] H.M. James, E. Guth, Theory of elastic properties of rubber, J. Chem. Phys. 11 (1969) 155–181.
[15] R.L. Jernigan, P.J. Flory, Distribution ffunction for chain molecules, J. Chem. Phys. 50 (1969) 4185–4200.
[16] A. Wineman, Some results for generalized neo-Hookean elastic materials, Int. J. Non-linear Mech. 10 (2005) 271–279.
[17] F.B. Millard, On constitutive models for limited elastic molecular based materials, Math. Mech. Solids 13 (2008) 375–387.
[18] P. Steinmann, M. Hossain, G. Possart, Hyperelastic models for rubber-like materials: consistent tangent operators and suitability for treloar's data, Arch. Appl. Mech. (2012).
[19] G. Marckmann, E. Verron, Comparison of hyperelastic models for rubber-like materials, Rubber Chem. Technol. 79 (2006) 835–858.
[20] A.N. Gent, A new constitutive relation for rubber, Rubber Chem. Technol. 69 (1996) 59–61.
[21] E. Pucci, G. Saccomandi, A note on the gent model for rubber-like materials, Rubber Chem. Technol. 75 (2002) 839–851.
[22] T. Beda, Reconciling the fundamental phenomenological expression of the strain energy of rubber with established experimental facts, Polym. Phys. 43 (2005) 125–134.
[23] K.C. Valanis, R.F. Landel, The strain-energy function of a hyperelastic material in terms of the extension ratios, J. Appl. Phys. 8 (1967) 2997–3002.
[24] A. Nguessong-Nkenfack, Modeling of rubber materials with a new hybrid isotropic hyperelastic density, Theory and finite element implementation (Ph. D. thesis), University of Ngaoundere and University of Technology of Belfort-Montbeliard, 2015.
[25] A. Nguessong-Nkenfack, T. Beda, F. Peyraut, A new based errors approach to approximate the inverse langevin function, Rheol. Acta 53 (2014) 585–591.
[26] L.R.G. Treloar, Stress–strain data for vulcanized rubber under various types of deformation, Trans. Faraday Soc. 40 (1944) 59–70.
[27] O.H. Yeoh, D.P. Fleming, A new attempt to reconcile the statistical and phenomenological theories of rubber elasticity, J. Polym. Sci.: Part B: Polym. Phys. 35 (1997) 1919–1931.
[28] L.C.S. Nunes, D.C. Moreira, Simple shear under large deformations: experimental and theoretical analyses, Eur. J. Mech. A/Solids 42 (2013) 315–322.
[29] R.S. Rivlin, D.W. Saunders, Large elastic deformation of isotropic materials – VII. Experiments on the deformation rubber, Philos. Trans. R. Soc. 243 (1951) 251–288.
[30] P. Ciarlet, Mechanical Elasticity: Three Dimensional Elasticity, 1988.
[31] F. Peyraut, Z.-Q. Feng, Q.-C. He, N. Labed, Robust numerical analysis of homogeneous and non-homogeneous deformations, Appl. Numer. Math. 59 (2009) 1499–1514.
[32] L.R.G. Treloar, The elasticity and related properties of rubbers, IOP Sci. Rep. Prog. Phys. 36 (1973) 755–826.
[33] R.C. Ball, M. Doi, S.F. Edwards, M. Warner, Elasticity of entangled networks, Polymer 122 (1981) 1010–1016.
[34] J.E. Mark, F. Horkay, G.B. Mckenna, Physical Property of Polymer Handbook, 1984.
[35] C.M. Boyce, E.M. Arruda, Constitutive models of rubber elasticity: a review, Rubber Chem. Technol. 73 (2000) 505–523.
[36] L.C.S. Nunes, Mechanical characterization of hyperelastic polydimethyl-siloxane by simple shear test, Mater. Sci. Eng. 528 (2011) 1799–1818.
[37] L.R.G. Treloar, The Physics of Rubber Elasticity, third edition, 1975.
[38] A. Cohen, A pade approximant to the inverse Langevin function, Rheol. Acta 30 (1991) 270–273.
[39] M. Puso, Mechanistic constitutive models for rubber elasticity and viscoelasticity (Ph.D. thesis), University of California Davis, 2003.
[40] L.R.G. Treloar, The photoelastic properties of short chain molecular networks, Trans. Faraday Soc. 50 (1954) 881–896.
[41] M. Itskov, R. Dargazang, K. Hornes, Taylor materials of the inverse function with application of the langevin function, Math. Mech. Solids 17 (2011) 693–701.
[42] W.H. Han, F. Horkay, G.B. Mckenna, Mechanical and swelling behavior of rubber: a comparison of some molecular models with experiment, Math. Mech. Solids 4 (1999) 139–167.
[43] H. Khajehsaeid, R. Arghdabadi, R. Naghdabadi, A hyperelastic constitutive model for rubber-like materials, Eur. J. Mech. A/Solids 38 (2013) 144–151.
[44] T. Beda, Y. Chevalier, Non-linear approximation method by an approach in stages, Comput. Mech. 32 (2003) 177–181.